analytical chemistry

Article

pubs.acs.org/ac

Nanoscaled Porphyrinic Metal–Organic Frameworks for Electrochemical Detection of Telomerase Activity via Telomerase Triggered Conformation Switch

Pinghua Ling, Jianping Lei,* and Huangxian Ju

State Key Laboratory of Analytical Chemistry for Life Science, School of Chemistry and Chemical Engineering, Nanjing University, Nanjing, Jiangsu 210023, P. R. China

Supporting Information

ABSTRACT: In this work, we designed a nanoscaled porphyrinic metal–organic framework (PorMOF) with iron porphyrin as linker and zirconium ion as node for electrochemical detection of telomerase activity. The as-prepared PorMOF was characterized with scanning electron microscopy, powder X-ray diffraction, and spectroscopic techniques and demonstrated excellent electrocatalytic activity toward O_2 reduction. Sequentially, the functionalization of PorMOF with streptavidin results in a water-stable electrochemical tracer for detection of telomerase. Upon the telomerase-triggered extension, the assistant DNA 1 (aDNA1)–assistant DNA 2 (aDNA2) duplex could switch into a hairpin structure, and thus, the aDNA2 was released and then hybridized with the capture DNA. Therefore, the PorMOF@SA tracer could be introduced on the electrode surface via biotin–streptavidin recognition, leading to the strong electrochemical signal for readout. The developed approach displayed desirable dynamic range and limitation of detection down to 30 HeLa cells mL^{-1}. The telomerase activity was 2.2×10^{-11} IU in a single HeLa cell with good reproducibility and stability. The nanoscaled porphyrinic MOF provided a powerful platform for electrochemical signal transduction and had a promising application in the determination of various biomolecules.

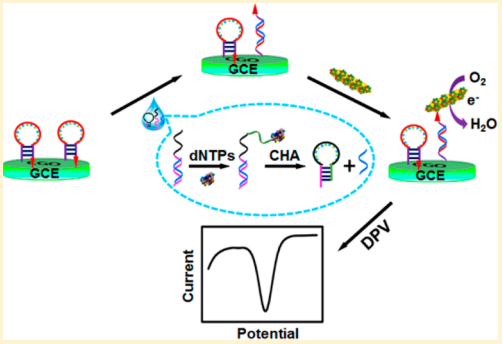

Telomeres with repeating sequences ((TTAGGG)n) are critical elements of eukaryotic chromosomes to protect the inherent genetic material.[1,2] Since the activation of telomerase results in the indefinite deviation of the cancer cells,[3,4] telomerase activity is considered as a significant parameter for early stage cancer diagnosis, prognosis, and the pathogenesis of disease.[5,6] From the discovery of telomerase, several analytical methods have been used to detect the activity of telomerase.[7,8] Conventionally, the polymerase chain reaction (PCR)-based telomeric repeat amplification protocol was the method most frequently used for analysis of telomerase activity due to its merit of high sensitivity.[9] Recently, several PCR-free approaches have been developed, such as colorimetry,[10−14] surface plasmon resonance,[15] fluorescence,[16,17] chemiluminescence,[18] electrochemical detection,[19−21] and electrochemiluminescence[22,23] for the detection of telomerase and its related biological research. In particular, electrochemical methods demonstrate some advantages for practical use due to the easy miniaturization and high sensitivity.[24] For example, an electrochemical sensitive telomerase biosensor was developed on the basis of horseradish peroxidase-catalyzed tetramethylbenzidine oxidation using a spired DNA tetrahedron telomere strand primer.[25] A simple electrochemical sensor based on the electrocatalysis of platinum nanoparticle toward $NaBH_4$ oxidation is constructed to detect the telomerase activity.[21] Although the above signal probes provide the large electrochemical signal for readout, the exogenous redox probes could block the application in biological systems. Therefore, it is urgent to develop a catalysis system with the endogenous redox substrate for producing an amplified electrochemical signal in the bioassay.

Metal–organic frameworks (MOFs) as a new class of highly ordered crystalline coordination polymers have fascinating structures such as permanent porosity, high surface area, open cavities, and a high degree of synthetic tunability for storage, separations, sensors, size- and shape-selective catalysis, and nanoscale reactors.[26−30] To develop porous MOFs as platforms for biomimetic catalysis, porphyrinic ligands have been extensively explored because of their multifunctionality.[31−33] The rigid structures of porphyrinic MOF (PorMOF) with high surface area and porosity can not only make each porphyrin accessible by substrates but also prevent the dimerization of reaction centers.[34] The microsized porphyrin-based MOFs have been widely used in biomimetic catalysis,[35,36] photodynamic therapy,[37−39] sensors,[40,41] and electrocatalysts.[42,43] The nanoscaled MOF material in the electrochemical biosensor could be more suitable as a signal transduction platform for electro-

Received: August 11, 2016
Accepted: October 11, 2016
Published: October 11, 2016

DOI: 10.1021/acs.analchem.6b03131
Anal. Chem. 2016, 88, 10680−10686

Scheme 1. Schematic Illustration of (A) the Preparation of Nanoscaled PorMOF and (B) the Electrochemical Detection Strategy for Telomerase Activity via a Telomerase Triggered Conformation Switch

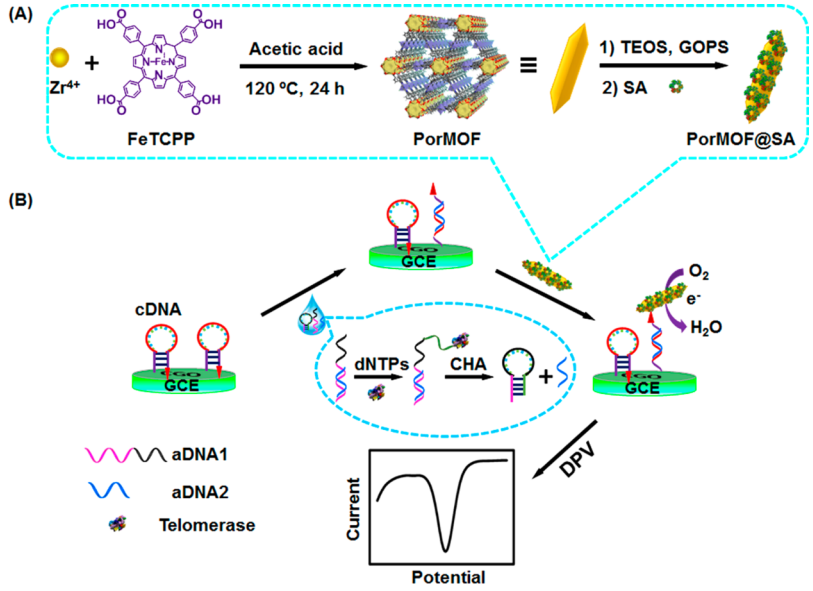

catalytic reduction of oxygen as endogenous signal to detect telomerase activity.

Here, integrating the electrocatalysis of nanoscale PorMOF toward oxygen reduction and the telomerase triggered conformation switch, a simple and reliable strategy is developed for detection of telomerase activity (Scheme 1). The signal nanoprobe was prepared using porphyrin as linker and zirconium ion as node and sequentially functionalized with streptavidin (SA) as recognition element. Because of the steric block, the nanoprobe was inhibited to interact with the immobilized biotin end labeled at the 5′ end of hairpin capture DNA (cDNA) on the electrode surface, as noted as the "closed" state. Upon the telomerase-triggered extension, the assistant DNA 1 (aDNA1) in duplex could be extended to fold to a hairpin structure in the presence of dNTP mixture and telomerase. Thus, the assistant DNA 2 (aDNA2) could be released and then hybridized with the cDNA, resulting in the "open" state. Afterward, through the biotin−streptavidin recognition, the PorMOF@SA nanoprobe was introduced to the electrode surface, leading to an enhanced current of electrocatalytic reduction toward oxygen for readout. Therefore, the biosensor could detect telomerase with a detection limit of 30 cell mL^{-1} and evaluate the telomerase activity even in single HeLa cancer cell. Various other cell lines were also tested for distinguishing the telomerase activity. The porphyrinic MOF provides an excellent signal transduction platform for detecting the various analytes and has great potential in the bioassay.

EXPERIMENTAL SECTION

Materials and Reagents. Zirconium chloride ($ZrCl_4$), acetic acid, dimethylformamide (DMF), (3-glycidyloxypropyl) trimethoxysilane ($C_9H_{20}O_5Si$, GOPS), *o*-phenylenediamine (o-PD), ferrocenediacetic acid (Fc), tetramethoxysilane (TEOS), 1-(3-(dimethylamino)propyl)-3-ethylcarbodiimide hydrochloride (EDC, ≥98%), streptavidin (SA), glycerol, 3-[(3-cholamidopropyl)dimethylammonio]-1-propanesulfonic acid (CHAPS), *N*-hydroxysuccinimide (NHS), ethylene glycol bis(aminoethyl ether)-*N*,*N*,*N*′,*N*′-tetraacetic acid (EGTA), and Tween 20 were obtained from Sigma-Aldrich Inc. (USA). Carboxylic graphene oxide (CGO, >99.8%) was purchased from Nanjing XFNano Materials Tech Co. Ltd. (Nanjing, China). Iron(III) meso-5,10,15,20-tetrakis(4-carboxyphenyl)porphyrin chloride (FeTCPP) was obtained from J&K Scientific Ltd. (China). The deoxynucleotide solution mixture (dNTPs) was purchased from Sangon Inc. (Shanghai, China). The telomerase ELISA kit containing a bottle of telomerase standard solution (80 IU L^{-1}), HeLa cell (Human cervix adenocarcinoma), HaCaT (immortalized human epidermal cells), HePG2 (human liver cancer cells), U87 (human glioma cell line), MCF-7 (human breast cancer cells), and CEM (acute lymphocytic leukemia cell) were from KeyGen Biotech. Co. Ltd. (Nanjing, China). Buffer solutions employed in this work were prepared as follows: 10 mM Tris−HCl containing 1.0 M NaCl (pH 7.4) was prepared as oligonucleotide stock solution and hybridization solution, and all other buffers (DNA immobilizing, electrode washing, and electrolyte solution) were prepared with 25 mM phosphate buffer saline (PBS) containing 25 mM NaCl. All DNA oligonucleotides were synthesized by Sangon Inc. (Shanghai, China) with the sequences as follows:

Assistant DNA 1 (aDNA1): 5′-GCAGCCCCTAACCCTAA-CCCTAA*AATCCGTCGAGCAGAGTT*-3′

Assistant DNA 2 (aDNA2): 5′-GTTAGGGGCTGCGTC-3′

Capture DNA (cDNA): 5′-NH_2-AAAAAAAAAATTCCTA-GACGCAGCCCCTAACTAGGAA-biotin-3′

The italic letters represent the telomere strand primer sequences. Oligonucleotides were heated to 90 °C for 5 min and then naturally cooled down to room temperature.

Apparatus. Scanning electron microscopy (SEM) images were taken on an S-4800 scanning electron microscope (Hitachi, Japan) integrated with EDX allowing one to perform qualitative and quantitative chemical analysis and image capture. Powder X-ray diffraction (PXRD) experiments were operated on a Bruker D8 Advance X-ray powder diffractometer at 40 kV and 40 mA (Cu Kα radiation, λ = 1.5418 Å). UV−vis spectra were carried out on a UV-3600 UV−vis−NIR spectrophotometer (Shimadzu Co., Kyoto, Japan). After

DOI: 10.1021/acs.analchem.6b03131
Anal. Chem. 2016, 88, 10680−10686

outgassing for 6 h at 60 °C, nitrogen sorption measurements were conducted with 50 mg of sample using a Micromeritics ASAP2020 at 77 K. The infrared spectra were obtained on a Vector 22 Fourier transform infrared (FT-IR) spectrometer (Bruker Optics, Germany). Cyclic voltammetry (CV) and differential pulse voltammograms (DPV) were carried out on a CHI 660D electrochemical workstation (Shanghai CH Instruments, China) at room temperature (~25 °C). The three-electrode system includes glassy carbon electrode (GCE) as the working electrode, saturated calomel electrode (SCE) as the reference, and platinum wire as the counter electrode. DPV was recorded in 25 mM PBS (pH 7.4) solution containing 25 mM NaCl at a potential range from 0.2 to −0.8 V with a modulation amplitude of 50 mV and a scan rate of 50 mV s^{-1}. The current value was obtained from the subtraction of the background.

The 10% native polyacrylamide gel electrophoresis (PAGE) was performed in 5× Tris-Borate-EDTA (TBE) buffer at 90 V for 90 min. After ethidium bromide staining, the gel was scanned with Molecular Imager Gel Doc XR (BIO-RAD, USA).

Preparation of PorMOF and PorMOF@SA Conjugate. The PorMOF was prepared according to the reported method with some modifications.[44] Typically, $ZrCl_4$ (15 mg), FeTCPP (20 mg), and acetic acid (0.4 mL) in 2 mL of DMF were ultrasonically dissolved in a 20 mL pyrex vial, followed by heating at 120 °C for 24 h. After cooling to room temperature, the dark brown material was obtained via centrifugation, washed with DMF, and then dried under vacuum at 60 °C for 24 h for further use.

Prior to use, the PorMOF was coated with TEOS and then 5% GOPS (v/v) to get the epoxy-functionalized PorMOF.[43] The PorMOF@SA was obtained via the covalent interaction between NH_2 groups of SA and epoxy groups on the PorMOF. In brief, 20 μL of SA (1 mg mL^{-1}) was injected into 100 μL of the epoxy-functionalized PorMOF aqueous solution (1 mg mL^{-1}) and slightly stirred for 12 h at 4 °C. The light brown material was obtained via centrifugation at 10 000 rpm and washed with 10 mM Tris−HCl containing 1.0 M NaCl (pH 7.4). The PorMOF@SA was redispersed in 10 mM Tris−HCl (pH 7.4) and stored at 4 °C for further use.

Cell Culture and Telomerase Extraction. HeLa, HaCaT, HePG2, and U87 cells were grown in Dulbecco's minimal essential (DMEM) medium supplemented with 10% fetal bovine serum (FBS); MCF-7 and CEM were cultured in Roswell Park Memorial Institute (RPMI 1640) medium 1640. All the cells were maintained at 37 °C in a humidified atmosphere (95% air and 5% CO_2) with logarithmic growth. Prior to any experiments, cells were counted using a Beckman cell counter.

About 10^7 cells in 1 mL of cell culture medium were transferred into a 1.5 mL EP tube and washed twice with ice-cold PBS (0.1 M, pH 7.4) by centrifugation at 2000 rpm for 5 min at 4 °C. The cells were resuspended in 200 μL of ice-cold CHAPS lysis buffer (10 mM Tris−HCl, pH 7.5, 1 mM $MgCl_2$, 1 mM EGTA, 0.1 mM phenylmethylsulfonyl fluoride, 5 mM mercapto ethanol, 0.5% CHAPS, 10% glycerol) and kept for 30 min in an ice bath. The lysate was centrifuged at 12 000 rpm for 20 min at 4 °C. The resulting extract was carefully frozen at −80 °C or used immediately. For the control experiment, the telomerase extract was heat-treated at 95 °C for 10 min prior to detection.

Construction of Biosensor and Electrochemical Detection. For the telomerase extension reaction, 10 μL of aDNA1−aDNA2 duplex, 20 μL of telomerase reaction solution containing 10 μL of telomerase extracts or standard telomerase, and 2 mM dNTPs in 1× TRAP buffer (20 mM Tris−HCl pH 8.3, 1.5 mM $MgCl_2$, 63 mM KCl, 0.005% Tween 20, 1 mM EGTA, BSA 0.1 mg mL^{-1}) were incubated at 37 °C for 150 min to allow the extension reaction by telomerase to occur. The resulting mixture was ready to use in the next electrochemical experiment.

The GCEs were twice polished with a slurry of Al_2O_3 powder (1.0 and 0.05 μm) on chamois leather, followed by ultrasonic cleaning with deionized water and drying at room temperature. After coating 5 μL of 1 mg mL^{-1} CGO in aqueous solution, the electrode was treated with the mixture of 400 mM EDC and 100 mM NHS (20 μL) for 30 min. The electrode was extensively washed and then exposed to 0.5 μM cDNA in 10 mM Tris−HCl containing 1.0 M NaCl (pH 7.4) for 4 h. The cDNA modified electrode was then incubated with the above mixture including the telomerase extension product for 60 min. Finally, the resulting electrode was immersed in 1.0 mg mL^{-1} PorMOF@SA solution at 37 °C for 45 min. After being washed, the biosensor was determined with CV and DPV in 0.1 M, pH 7.4 O_2-saturated PBS.

RESULTS AND DISCUSSION

Characterization of PorMOF and PorMOF@SA. The PorMOF was prepared with FeTCPP as linker and Zr as node via solvothermal reaction. From SEM images of PorMOF, a uniform and hexagonal needle-shape was observed with a 600 nm length and the width of each side of the hexahedron was ~100 nm (Figure 1A), which was attributed to acetic acid being

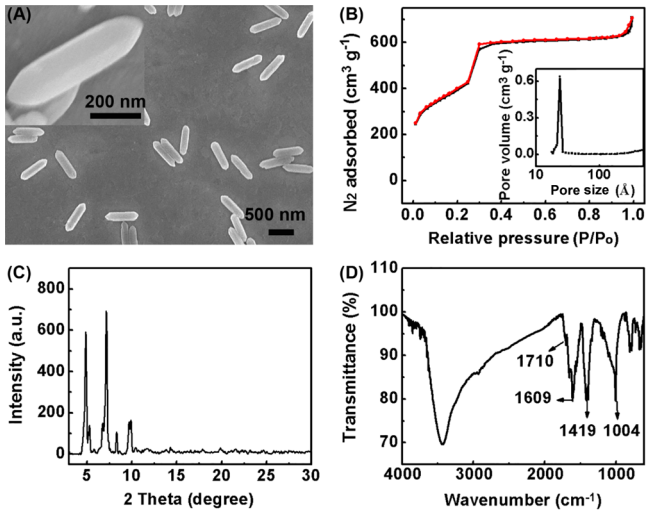

Figure 1. (A) SEM images and (B) nitrogen adsorption−desorption of nanoscaled PorMOF. Inset: Enlarged morphology and pore size distribution with N_2 at 77 K for (A) and (B), respectively. (C) PXRD and (D) FT-IR spectrum of PorMOF.

a weak acid and thus facilitating the formation of an entropically favored product.[45] In addition, these EDX images clearly show the presence of Fe and Zr with a uniform distribution (Figure S1), and the EDX analysis shows 1:11 of the atomic ratio of Fe to Zr (Table S1). These results demonstrate the successful synthesis of nanoscaled PorMOF, providing an efficient platform as mimetic catalyst.

The permanent porosity and pore size of PorMOF are confirmed by nitrogen-sorption measurements at 77 K. As shown in Figure 1B, the type-IV isotherms of PorMOF were

DOI: 10.1021/acs.analchem.6b03131
Anal. Chem. 2016, 88, 10680−10686

observed with a steep increase at the point of P/P_0 = 0.3, suggesting its mesoporosity. The Brunauer–Emmett–Teller (BET) surface area of nanoscaled PorMOF was obtained to be 1658 m^2 g^{-1} with the porosity of ~0.99 cm^3 g^{-1}, which is beneficial to its application as a catalytic system. The pore size was mainly around 2.4 nm (Figure 1B), which is consistent with the isotherm data. The structure of PorMOF was further validated with PXRD (Figure 1C). The PXRD curve shows the peaks at 4.86°, 7.02°, 8.30°, and 9.63°, which can be indexed to (−220), (410), (500), and (−150) of the spindle hexahedron geometry (JCPDF card number: 52–2360), respectively. The characteristic FT-IR peaks were observed for porphine ring skeleton absorption at 1710 (w), 1609 (s), 1368 (s), 1419 (vs), the O–H stretch at 1004 (s), and benzene rings at 871 (w) and 779 (m) cm^{-1} in FeTCPP, respectively (Figure 1D), indicating that FeTCPP was involved in the frameworks.

After functionalization of PorMOF with SA, some agglomerates were observed on the surface of PorMOF (Figure 2A).

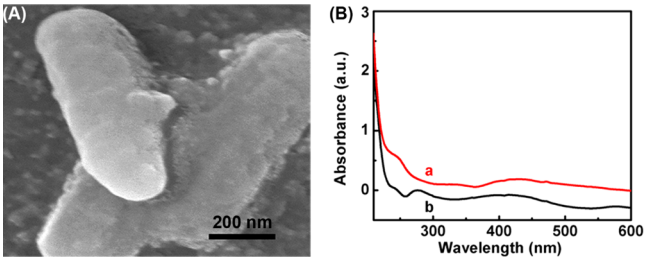

Figure 2. (A) SEM image of PorMOF@SA. (B) UV–vis absorption spectra of PorMOF (a) and PorMOF@SA (b).

However, the structure of PorMOF was maintained. UV–vis absorption spectra were employed to identify the formation of PorMOF@SA (Figure 2B). From the UV–vis spectra, a new Soret absorption of PorMOF@SA appeared at 278 nm in comparison with that of pure PorMOF, indicating the successful loading of the SA protein on the PorMOF surface.

Electrocatalysis of PorMOF. Figure 3A showed the electrocatalytical behaviors at different electrodes in pH 7.4 O_2-saturated PBS. A reduction peak was observed at around −0.60 V in O_2-saturated PBS at the CGO/GCE (curve a). Compared with that in N_2-saturated PBS (curve b), the reduction peak of PorMOF/CGO/GCE shifts to −0.32 V in O_2-saturated PBS (curve c), which is attributed to the electrocatalytic reduction of O_2. During the process, FeTCPP in the PorMOF was first reduced to iron(II) species and then back to the initial state by means of a chemical reaction with O_2. Since the SA protein blocked access to catalytic sites, the PorMOF@SA/CGO/GCE showed a smaller current response than that of PorMOF/CGO/GCE in O_2-saturated PBS (curve d). The highly efficient electrocatalysis of the nanoscaled PorMOF toward O_2 as the endogenous redox substrate provides the amplified electrochemical signal for readout.

Furthermore, the catalytic properties of FeTCPP, hemin, PorMOF, and horseradish peroxidase (HRP) at different temperatures and pH values were investigated in Figure 3B,C. Compared with a 49.5% loss of the catalytic activity of HRP at 60 °C, the PorMOF framework demonstrated little vulnerability to the high temperature (Figure 3B). When HRP was kept in alkaline solution for 1 h, the catalytic activity of HRP was lost by 41%. Meanwhile, the PorMOF framework exhibited good stability (Figure 3C). These results indicate that the prepared PorMOF framework had much better stability than HRP in broad detection conditions.[46] Moreover, to test the biomimetic catalytic activity, PorMOF was employed in the oxidation of o-PD and Fc (Figures S2 and S3). Kinetic experiments revealed that the PorMOF exhibited excellent peroxidase-like catalytic activity.

Feasibility of the Sensor. The DPV was employed to investigate the feasibility of the sensor in response to telomerase activity in Figure 4A. When the cDNA modified

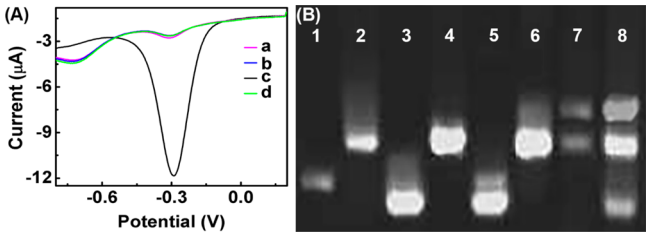

Figure 4. (A) DPV responses of PorMOF@SA at cDNA modified GCE after incubation in PBS containing dNTPs (a), (a) plus aDNA1–aDNA2 duplex (b), (b) plus the extract (c), and (b) plus the heated extract (d). Scan rate: 50 mV s^{-1}. (B) PAGE analysis of 10 μM aDNA1 (lane 1), aDNA2 (lane 2), cDNA (lane 3), aDNA1–aDNA2 duplex (lane 4), aDNA1 + cDNA (lane 5), aDNA2 + cDNA (lane 6), aDNA1–aDNA2 duplex + cell extract (lane 7), and aDNA1–aDNA2 duplex + cDNA + cell extract (lane 8) in the presence of dNTPs.

GCE was incubated in PBS containing dNTPs (curve a) and dNTPs + aDNA1–aDNA2 duplex (curve b) and then PorMOF@SA, the sensor showed the small peak current at around −0.28 V, which is attributed to the nonspecific interaction of the PorMOF@SA on the electrode surface. Upon the addition of the active telomerase into the mixture of aDNA1–aDNA2 duplex and dNTP, the biosensor demonstrated the strong electrochemical signal (curve c). This phenomenon can be described due to the aDNA1–aDNA2

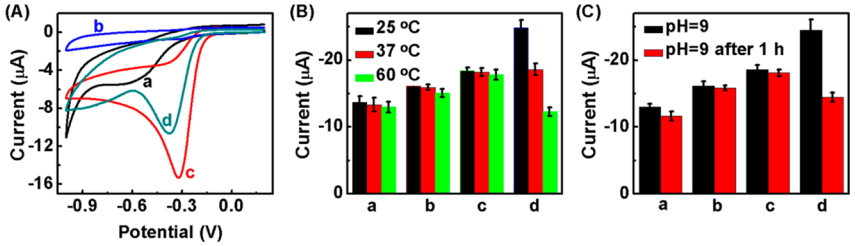

Figure 3. (A) CVs of CGO/GCE (a), PorMOF/CGO/GCE (c), and PorMOF@SA/CGO/GCE (d) in O_2-saturated PBS and PorMOF/CGO/GCE in N_2-saturated PBS (b). Scan rate: 50 mV s^{-1}. Current responses of 0.1 mg mL^{-1} FeTCPP (a), Hemin (b), PorMOF (c), and HRP (d) to (B) different temperatures for 0.5 h and (C) alkaline solution for 1 h in the detection solution containing 10 mM o-PD and 8.0 mM H_2O_2.

DOI: 10.1021/acs.analchem.6b03131
Anal. Chem. 2016, 88, 10680–10686

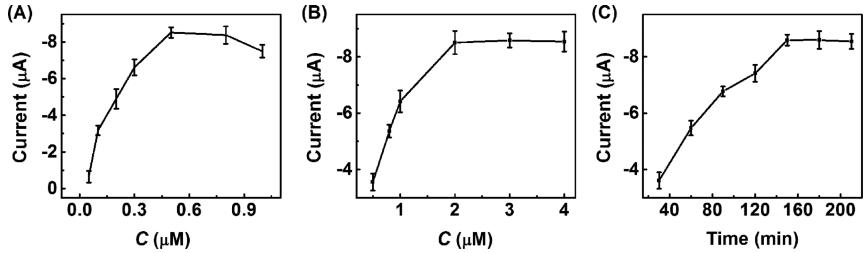

Figure 5. Effects of (A) concentration of cDNA, (B) concentration of aDNA1−aDNA2 duplex, and (C) incubation time for telomerase extension reaction on electrocatalytic current of the biosensor toward O_2 reduction.

duplex switching to hairpin structure when the telomerase extension product of aDNA1 is formed, and thus, the aDNA2 is released to hybridize with cDNA, resulting in the "open" state to bind with PorMOF@SA for electrocatalytic reduction of O_2 as detectable electrochemical signal. As a control, when the aDNA1−aDNA2 duplex is treated with the heat-treated cell extract (curve d), the electrochemical signal is still small, indicating the heat-treated telomerase loses its activity.

In order to further verify the feasibility of this method, the gel electrophoresis was employed (Figure 4B). aDNA1 (lane 1), aDNA2 (lane 2), cDNA (lane 3), and aDNA1−aDNA2 duplex (lane 4) demonstrated the single migration band under the same condition. After incubating aDNA1 and cDNA, two bands are obtained at the positions corresponding to individual aDNA1 and cDNA (lane 5), suggesting no hybridization between aDNA1 and cDNA. When aDNA2 was incubated with cDNA, a new band with low migration rate appeared on the gel, indicating aDNA2 was hybridized with cDNA (lane 6). After incubation of aDNA1−aDNA2 duplex with the dNTPs and telomerase extract, there are two bands on the gel (lane 7), corresponding to the positions of telomerase extension product of aDNA1 and the aDNA2, respectively. Following with the addition of cDNA, a bright band was obviously observed with the middle migration rate (lane 8), corresponding to the band of aDNA1−aDNA2, which is consistent with lane 6. These results suggested that the biosensor is highly feasible in the detection of telomerase activity.

Optimization of Detection Conditions. In order to develop the biosensor with high sensitivity, several parameters such as the concentration of cDNA, the concentration of the aDNA1−aDNA2 duplex, and the incubation time for telomerase extension reaction were investigated. With the increasing cDNA concentration, the current reached the plateau at 0.5 μM and then decreased (Figure 5A), since more cDNA on the electrode surface could generate steric hindrance. Thus, 0.5 μM cDNA was utilized to modify the electrode. The effect of concentration of the aDNA1−aDNA2 duplex is also optimized (Figure 5B). With the increase of the aDNA1−aDNA2 concentration, DPV peak current intensities were enhanced at first and then reached a plateau at 2 μM, which was chosen as the optimal concentration. The incubation time for telomerase extension reaction was also investigated (Figure 5C). The DPV peak current values increased with time and then reached the plateau at 150 min. As a result, a telomerase extension reaction time of 150 min was chosen as the optimal experimental time.

Detection of Telomerase Activity. To demonstrate the sensitivity of the proposed method, the HeLa cells were used as a model for sensitive quantification of telomerase. The electrochemical signals in response to the different concentrations of HeLa cells were evaluated with DPV measurements under the optimized conditions. As shown in Figure 6, the results were obtained with the dynamic correlation between

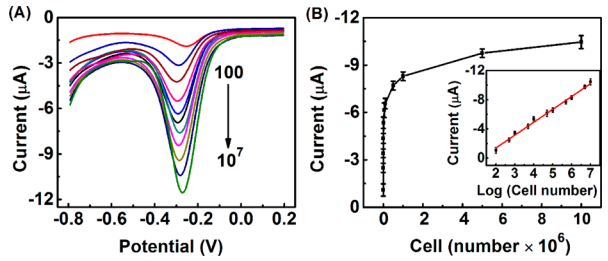

Figure 6. (A) DPV signals of a range of HeLa cell numbers: 10^2, 5×10^2, 10^3, 5×10^3, 10^4, 5×10^4, 10^5, 5×10^5, 10^6, 5×10^6, and 10^7 cells mL^{-1}. (B) Dependence of DPV peak currents on HeLa cell concentrations. Inset: Calibration curve.

DPV peak current at −0.28 V and telomerase activity from 10^2 to 10^7 HeLa cells mL^{-1}. With the increasing HeLa cells concentrations (Figure 6A), more aDNA2 was released, resulting in more cDNA that could bind with PorMOF@SA for electrocatalysis toward O_2 reduction. The response of telomerase activity was quantified by the DPV peak current at −0.28 V in Figure 6B. Moreover, the peak currents exhibited a good proportion to the logarithm of the HeLa cell concentration in the range from 10^2 to 10^7 HeLa cells mL^{-1} (inset in Figure 6B). The detection limit of 30 HeLa cells mL^{-1} was calculated at the S/N = 3, which was lower than 1000 HeLa cells mL^{-1} of the method based on electrochemical impedance spectroscopy.[47]

In order to estimate the reproducibility, ten independently prepared electrodes were used with the relative standard deviations (RSDs) of 4.8%. When stored at 4 °C for 10 days, the biosensor maintained 93.8% of the initial value. Further, to evaluate its repeatability, the RSDs (n = 3) of peak current intensities were 3.5%, 4.6%, and 4.1% in response to 500, 5000, and 10 000 HeLa cells. Under the optimal experimental condition, a standard curve was achieved by using different concentrations of telomerase (Figure S4). Therefore, the telomerase activity in a single HeLa cell was obtained to be 2.2×10^{-11} IU, which was less than 3.2×10^{-11} IU of the Au NPs probe in vivo system.[17]

Moreover, to ensure that it is a general and reliable method for telomerase detection, we challenged our system with different cell lines such as HaCat, U87, CEM, HEpG2, and MCF-7. The telomerase activity of each cell line was normalized to the activity of HeLa cells. Due to the lack of telomerase activity in normal cells and the heated extract, both HaCat cell and the heated extract sample did not show obvious electrochemical signal. However, the other cancer cell lines showed positive telomerase activity (Figure 7), which was

DOI: 10.1021/acs.analchem.6b03131
Anal. Chem. 2016, 88, 10680−10686

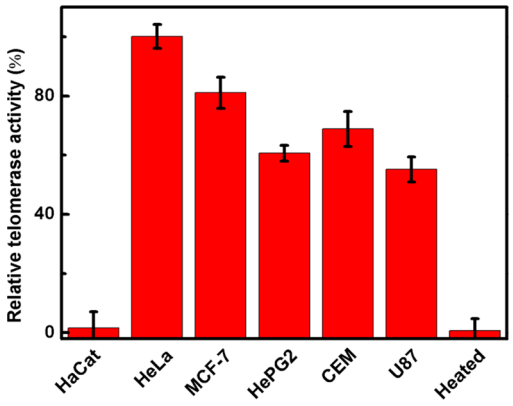

Figure 7. Solid-state electrochemical assay to analyze telomerase activities in different cell lines. All telomerase activity was normalized to HeLa cells. The cell extracts were equivalent to 2000 cells.

consistent with the previous results in extracts of two human cancer cells (MCF-7, HeLa).[24,48] The practical application of the biosensor was tested in serum samples from the patients without the requirement of sample pretreatment, except a dilution step. A total of 4 serum samples were measured, and the results are shown in Table S2. When spiking with standard telomerase to real serum samples, the analytical recoveries are from 96.1% to 107.5%, indicating good accuracy of this approach in determination of telomerase activity in real samples.

CONCLUSIONS

In summary, we successfully developed a nanoscaled PorMOF for electrochemical evaluation of telomerase activity via a target-triggered conformation switch. The nanoscaled PorMOFs were designed with porphyrin as both linker and electrocatalytic active site and thus demonstrated high electrocatalytic reduction of O_2 as an endogenous signal substrate and high stability with excellent peroxidase-like catalytic capacity in broad conditions. On the basis of the telomerase-triggered extension, the DNA duplex could switch into a hairpin structure, and thus, the signal probe was brought onto the electrode surface via SA–biotin biorecognition and led to an enhanced current for signal readout. This designed assay could detect telomerase activity as low as 30 HeLa cells with a detection range over 5 orders of magnitude and even detect the telomerase activity in a single HeLa cancer cell. Moreover, the method was PCR-free, enzyme-free, low cost, and without the requirement of additional separation steps. The nanoscaled porphyrinic MOF paves a new way for the detection of various analysts and has the potential applications in bioassays.

ASSOCIATED CONTENT

Supporting Information

The Supporting Information is available free of charge on the ACS Publications website at DOI: 10.1021/acs.analchem.6b03131.

Characterization of PorMOF, peroxidase-like activity, standard curve of enzymatic activity, and telomerase activity in human blood serum samples (PDF)

AUTHOR INFORMATION

Corresponding Author

*Phone/Fax: +86-25-89681922. E-mail: jpl@nju.edu.cn.

Notes

The authors declare no competing financial interest.

ACKNOWLEDGMENTS

This work was financially supported by the National Natural Science Foundation of China (21375060, 21135002, 21675084) and Priority development areas of the National Research Foundation for the Doctoral Program of Higher Education of China (20130091130005).

REFERENCES

(1) Cohen, S. B.; Graham, M. E.; Lovrecz, G. O.; Bache, N.; Robinson, P. J.; Reddel, R. R. *Science* **2007**, *315*, 1850–1853.
(2) Blackburn, E. H. *Cell* **2001**, *106*, 661–673.
(3) Patel, S. D.; Isalan, M.; Gavory, G.; Ladame, S.; Choo, Y.; Balasubramanian, S. *Biochemistry* **2004**, *43*, 13452–13458.
(4) Masutomi, K.; Yu, E. Y.; Khurts, S.; et al. *Cell* **2003**, *114*, 241–253.
(5) Lu, L. G.; Zhang, C.; Zhu, G. J.; Irwin, M.; Risch, H.; Menato, G.; Mitidieri, M.; Katsaros, D.; Yu, H. *Breast Cancer Res.* **2011**, *13*, R56.
(6) Zhou, X. M.; Xing, D. *Chem. Soc. Rev.* **2012**, *41*, 4643–4656.
(7) Hou, M.; Xu, D. W.; Björkholm, M.; Gruber, A. *Clin. Chem.* **2001**, *47*, 519–524.
(8) Niemeyer, C. M.; Adler, M.; Wacker, R. *Trends Biotechnol.* **2005**, *23*, 208–216.
(9) Reed, J. E.; Arnal, A. A.; Neidle, S.; Vilar, R. *J. Am. Chem. Soc.* **2006**, *128*, 5992–5993.
(10) Wang, J. S.; Wu, L.; Ren, J. S.; Qu, X. G. *Small* **2012**, *8*, 259–264.
(11) Duan, R. X.; Wang, B. Y.; Zhang, T. C.; Zhang, Z. Y.; Xu, S. F.; Chen, Z. F.; Lou, X. D.; Xia, F. *Anal. Chem.* **2014**, *86*, 9781–9785.
(12) Sharon, E.; Golub, E.; Niazov-Elkan, A.; Balogh, D.; Willner, I. *Anal. Chem.* **2014**, *86*, 3153–3158.
(13) Lou, X. D.; Zhuang, Y.; Zuo, X. L.; Jia, Y. M.; Hong, Y. N.; Min, X. H.; Zhang, Z. Y.; Xu, X. M.; Liu, N. N.; Xia, F.; Tang, B. Z. *Anal. Chem.* **2015**, *87*, 6822–6827.
(14) Wu, H.; Liu, Y. L.; Wang, H. Y.; Wu, J.; Zhu, F. F.; Zou, P. *Biosens. Bioelectron.* **2015**, *66*, 277–282.
(15) Sharon, E.; Freeman, R.; Riskin, M.; Gil, N.; Tzfati, Y.; Willner, I. *Anal. Chem.* **2010**, *82*, 8390–8397.
(16) Zuo, X. L.; Xia, F.; Patterson, A.; Soh, H. T.; Xiao, Y.; Plaxco, K. W. *ChemBioChem* **2011**, *12*, 2745–2747.
(17) Qian, R. C.; Ding, L.; Yan, L. W.; Lin, M. F.; Ju, H. X. *Anal. Chem.* **2014**, *86*, 8642–8648.
(18) Li, Y.; Li, X.; Ji, X. T.; Li, X. M. *Biosens. Bioelectron.* **2011**, *26*, 4095–4098.
(19) Liu, X. J.; Li, W.; Hou, T.; Dong, S. S.; Yu, G. H.; Li, F. *Anal. Chem.* **2015**, *87*, 4030–4036.
(20) Liu, J.; Lu, C. Y.; Zhou, H.; Xu, J. J.; Wang, Z. H.; Chen, H. Y. *Chem. Commun.* **2013**, *49*, 6602–6604.
(21) Ling, P. H.; Lei, J. P.; Jia, L.; Ju, H. X. *Chem. Commun.* **2016**, *52*, 1226–1229.
(22) Zhou, X. M.; Xing, D.; Zhu, D. B.; Jia, L. *Anal. Chem.* **2009**, *81*, 255–261.
(23) Wu, L.; Wang, J. S.; Feng, L. Y.; Ren, J. S.; Wei, W. L.; Qu, X. G. *Adv. Mater.* **2012**, *24*, 2447–2452.
(24) Wu, L.; Wang, J. S.; Ren, J. S.; Qu, X. G. *Adv. Funct. Mater.* **2014**, *24*, 2727–2733.
(25) Li, Y.; Wen, Y. L.; Wang, L. L.; Liang, W.; Xu, L.; Ren, S. Z.; Zou, Z. Y.; Zuo, X. L.; Fan, C. H.; Huang, Q.; Liu, G.; Jia, N. Q. *Biosens. Bioelectron.* **2015**, *67*, 364–369.
(26) Li, Q. W.; Zhang, W. Y.; Miljanić, O. Š.; Sue, C. H.; Zhao, Y. L.; Liu, L. H.; Knobler, C. B.; Stoddart, J. F.; Yaghi, O. M. *Science* **2009**, *325*, 855–859.
(27) Zhou, H. C.; Long, J. R.; Yaghi, O. M. *Chem. Rev.* **2012**, *112*, 673–674.
(28) Wu, H.; Gong, Q.; Olson, D. H.; Li, J. *Chem. Rev.* **2012**, *112*, 836–868.

DOI: 10.1021/acs.analchem.6b03131
Anal. Chem. 2016, 88, 10680–10686

(29) Nugent, P.; Belmabkhout, Y.; Burd, S. D.; Cairns, A. J.; Luebke, R.; Forrest, K.; Pham, T.; Ma, S. Q.; Space, B.; Wojtas, L.; Eddaoudi, M.; Zaworotko, M. J. *Nature* **2013**, *495*, 80−84.
(30) Gao, W. Y.; Chen, Y.; Niu, Y. H.; Williams, K.; Cash, L.; Perez, P. J.; Wojtas, L.; Cai, J. F.; Chen, Y. S.; Ma, S. Q. *Angew. Chem., Int. Ed.* **2014**, *53*, 2615−2619.
(31) Son, H. J.; Jin, S.; Patwardhan, S.; Wezenberg, S. J.; Jeong, N. C.; So, M.; Wilmer, C. E.; Sarjeant, A. A.; Schatz, G. C.; Snurr, R. Q.; Farha, O. K.; Wiederrecht, G. P.; Hupp, J. T. *J. Am. Chem. Soc.* **2013**, *135*, 862−869.
(32) Gao, W. Y.; Chrzanowski, M.; Ma, S. Q. *Chem. Soc. Rev.* **2014**, *43*, 5841−5866.
(33) Park, J.; Feng, D. W.; Yuan, S.; Zhou, H. C. *Angew. Chem., Int. Ed.* **2015**, *54*, 430−435.
(34) Feng, D. W.; Gu, Z. Y.; Li, J. R.; Jiang, H. L.; Wei, Z. W.; Zhou, H. C. *Angew. Chem., Int. Ed.* **2012**, *51*, 10307−10310.
(35) Chen, Y.; Hoang, T.; Ma, S. Q. *Inorg. Chem.* **2012**, *51*, 12600−12602.
(36) Zhao, M.; Ou, S.; Wu, C. D. *Acc. Chem. Res.* **2014**, *47*, 1199−1207.
(37) Park, J.; Jiang, Q.; Feng, D. W.; Mao, L. Q.; Zhou, H. C. *J. Am. Chem. Soc.* **2016**, *138*, 3518−3525.
(38) Lu, K. D.; He, C. B.; Lin, W. B. *J. Am. Chem. Soc.* **2014**, *136*, 16712−16715.
(39) Lu, K. D.; He, C. B.; Lin, W. B. *J. Am. Chem. Soc.* **2015**, *137*, 7600−7603.
(40) Jiang, H. L.; Feng, D. W.; Wang, K. C.; Gu, Z. Y.; Wei, Z. W.; Chen, Y. P.; Zhou, H. C. *J. Am. Chem. Soc.* **2013**, *135*, 13934−13938.
(41) Deibert, B. J.; Li, J. *Chem. Commun.* **2014**, *50*, 9636−9639.
(42) Ling, P. H.; Lei, J. P.; Zhang, L.; Ju, H. X. *Anal. Chem.* **2015**, *87*, 3957−3963.
(43) Ling, P. H.; Lei, J.; Ju, H. X. *Biosens. Bioelectron.* **2015**, *71*, 373−379.
(44) Liu, T. F.; Feng, D. W.; Chen, Y. P.; Zou, L. F.; Bosch, M.; Yuan, S.; Wei, Z. W.; Fordham, S.; Wang, K. C.; Zhou, H. C. *J. Am. Chem. Soc.* **2015**, *137*, 413−419.
(45) Feng, D. W.; Chung, W. C.; Wei, Z. W.; Gu, Z. Y.; Jiang, H. L.; Chen, Y. P.; Darensbourg, D. J.; Zhou, H. C. *J. Am. Chem. Soc.* **2013**, *135*, 17105−17110.
(46) Gao, L. Z.; Zhuang, J.; Nie, L.; Zhang, J. B.; Zhang, Y.; Gu, N.; Wang, T. H.; Feng, J.; Yang, D. L.; Perrett, S.; Yan, X. Y. *Nat. Nanotechnol.* **2007**, *2*, 577−583.
(47) Yang, W. Q.; Zhu, X.; Liu, Q. D.; Lin, Z. Y.; Qiu, B.; Chen, G. N. *Chem. Commun.* **2011**, *47*, 3129−3131.
(48) Xiao, Y.; Dane, K. Y.; Uzawa, T.; Csordas, A.; Qian, J. R.; Soh, H. T.; Daugherty, P. S.; Lagally, E. T.; Heeger, A. J.; Plaxco, K. W. *J. Am. Chem. Soc.* **2010**, *132*, 15299−15307.

DOI: 10.1021/acs.analchem.6b03131
Anal. Chem. 2016, 88, 10680−10686